Supplemental material for: Dislocation creep near the frictional-viscous transition in blueschist: experimental constraints

Hufford et al.

Correspondence to: ljhufford@alumni.colostate.edu

Included Tables in Supplement Folder:

Table S1: Lead corrections for the strain rate stepping experiments. The corrections were calculated by not rounding until the equivalent stresses were calculated. These stresses and strain rates were used for the lead corrections.

Table S2: Mechanical data with and without the lead corrections.

Table S3: Parameters used for EBSD thin section polishing.

S1. Sample Preparation

We took a MORB blueschist (Fig. S1) and produced glaucophane aggregates through a series of mineral separation techniques to obtain a powder with ~98% glaucophane powder with sieve fractions 63-355 μm, 75-90 μm, and a fine-grained powder crushed with a mortar and pestle (<63 μm, measured with EBSD, Fig. S2). A combination of the following techniques were used and repeated to purify the powder as much as possible before picking. After this exploratory exercise, we recommend the follow procedure to expediate the process in the future:

- Selfrag- disaggregation of rock pieces to various grain sizes
- Wilfley table- water table density separation
- Sieving
- Frantz magnetic separator
- Picking large grains and crushing (if applicable)
- Air sieving- higher precision and finer grain separation (if applicable)
- Typ-91 magnetic separator- higher precision mineral separation (if applicable)
- Heavy Liquid- methylene iodide density separation
- Picking- non-amphibole grains out of powder

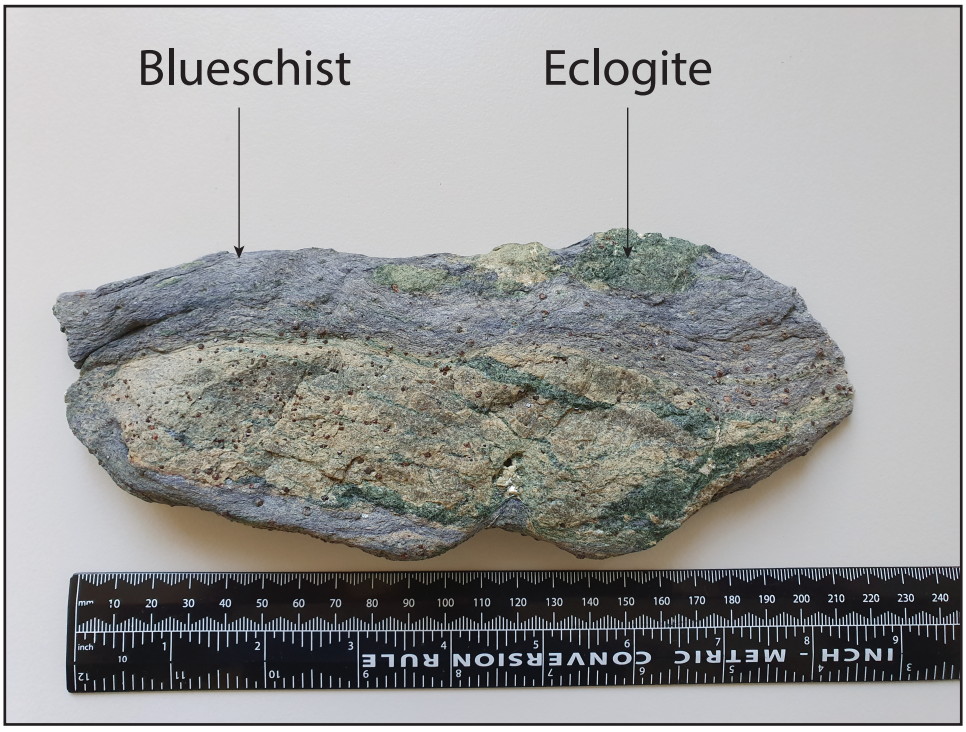

Figure S1: Hand sample where glaucophane aggregate powder originates from.

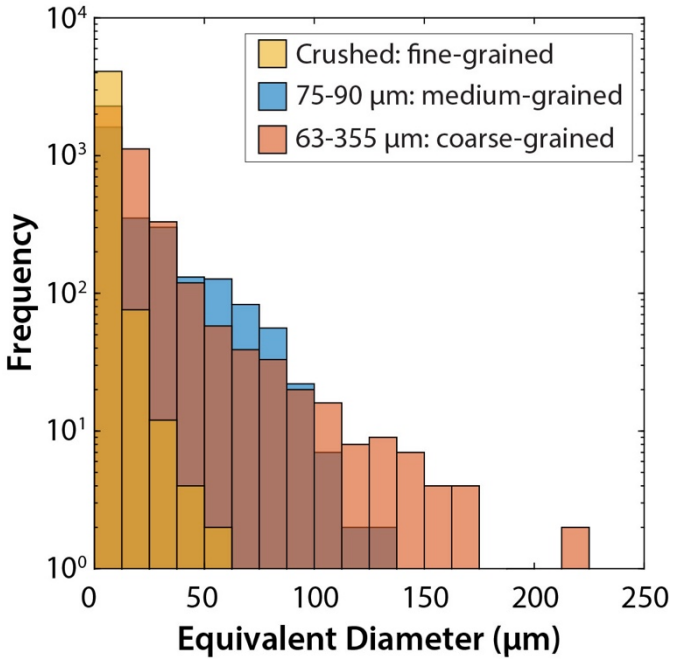

Figure S2: The starting grain size fractions from the hydrostatic samples were measured from EBSD data.

S2. Experimental Conditions and Microprobe

The timing for experimental conditions were constrained by the stability of glaucophane. We collected microprobe data to verify that the glaucophane did not chemically change during deformation experiments at 700°C and 1.0 GPa. Figure S3 shows microprobe data from a thin section of the hand sample and of a deformation experiment of an aggregate containing ~70-80% glaucophane conducted at 700°C and 1.0 GPa for ~4 days. The data show that the grains were still compositionally glaucophane (Leake et al., 1997) at the deformation conditions. The microstructures for several experiments conducted at temperatures of 725°C and higher show evidence for amphibole breakdown, visible through the development of exsolution textures. Exsolution textures were clearly visible in experiments lasting ~2 weeks and were not used to constrain the rheology of glaucophane. As a result, all experiments conducted at 725 and 750°C lasted no longer than 72 hours, to minimize any potential effect of amphibole breakdown on the rheology of our experiments. For the 750°C strain rate stepping experiment (LH045) that was conducted at ~3 days, exsolution textures were minor. These observations are consistent with the melting temperatures of glaucophane reported at ~1.5 GPa and ~1000K (~725°C) (Manthilake et al., 2021 and sources within).

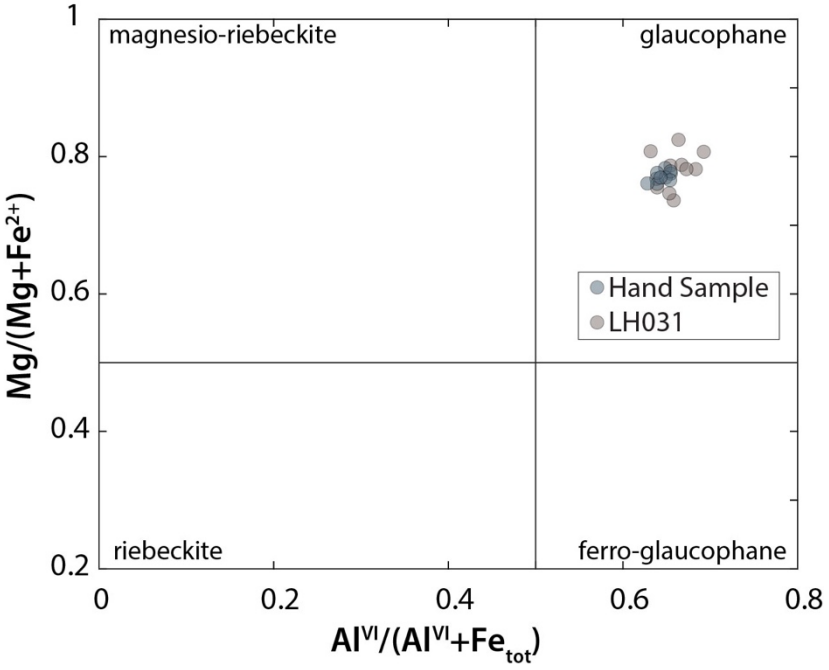

Figure S3: Electron microprobe analysis on a thin section from the original blueschist sample and a deformation experiment (LH031) conducted at 700°C and 1.0 GPa containing ~70-80% glaucophane. Both samples plot within the "Glaucophane" field of the Leake et al., 1997 classification scheme.

The microbprobe data were collected at ETH Zürich. Elements were acquired using analyzing crystals TAP (Si, Al), TAPH (Al, Ca), PETJ (Ca, Cr), PETL (K, Ti), and LIFH (Fe, Mn) crystals. All analyses were performed at 15 keV. The beam current was set to 20 nA with a beam size of 2 or 5 μm. All elements were measured for 30s on peak and the Mean Atomic Number (MAN) background correction (Donovan and Tingle, 1996) was applied using the software Probe for EPMA. Standardization was carried out using synthetic rutile (Ti), chromite (Cr), synthetic pyrolusite (Mn), albite (Si, Na), synthetic forsterite (Mg), anorthite (Al, Ca), microcline (K), and fayalite (Fe).

S3. Pb Corrections

Work has shown that rate-dependent friction can affect the stress during deformation experiments (Getsinger and Hirth, 2014; Proctor and Hirth, 2016; Okazaki and Hirth, 2020). Previous experimental studies have addressed this issue by performing lead stepping experiments to measure the effect of friction on stress so that it may be accounted for in data processing. We performed a lead-stepping experiment at 700°C before reaching the hit point. We deformed the lead piece at a reference rate and an order of magnitude above and below this reference rate. We show changes up to ~11 MPa above the reference rate and ~5 MPa below the reference rate (Fig. S4). We use an average of 8 MPa per order of magnitude change from the reference deformation rate by binning 8 MPa an order of magnitude above and below the strain rate of the first deformation step. We simplify this process by making the assumption that the change in stress is linear and apply a linear correction to the strain rate stepping experiments. Table S1 shows the binning process and Table S2 shows the data with and without the lead corrections.

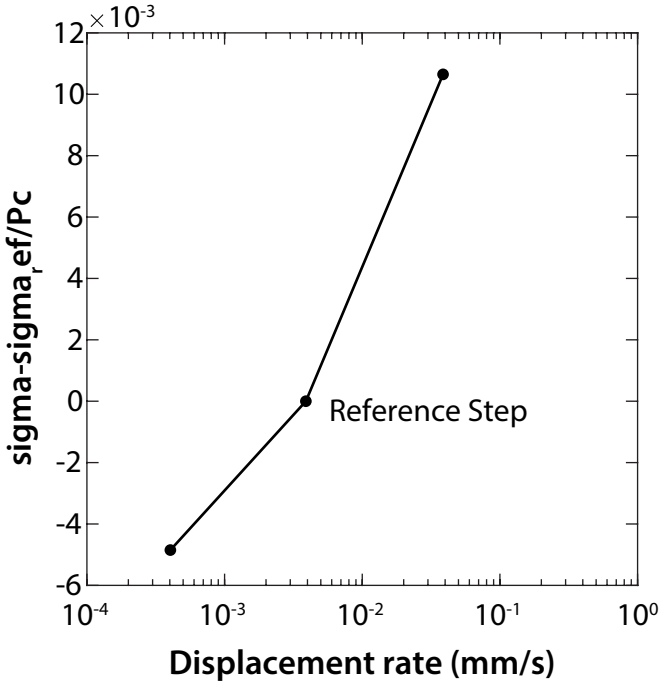

Figure S4: Plot of the Pb stepping experiment showing the range in stress over displacement rate.

S4. Electron Backscatter Diffraction (EBSD)

S4.1 EBSD Preparation and Methods

Thin sections were mechanically polished in a standard automated rotary polishing machine with water-based diamond solutions in different substrates accordingly to the Table S3. After each polishing step samples were carefully cleaned with running water, liquid soap and given an ultrasonic bath for 5 minutes. For the EBSD measurements, we coated all thin sections with 3 nm of C. Automated orientation mapping was performed with an acceleration voltage of 20 kV, beam current of 8 nA, working distance of 15 mm and stepsize of 100 nm. Due to the very poor indexation of fine-grained amphibole, we have used the Sensitivity mode of the EBSD camera (622x512 pixels), with manual gain of 1, frame averaging of 5 and >100 reflectors, reducing considerably the acquisition speed in favor of much better indexation rates. Basic post-acquisition cleaning up procedure was performed in Aztec 5.1, and included the removal of wild spikes (isolated 1-pixel "grain" with different orientation of the surrounding grain) and removal of zero solutions, the latter considering a minimum of 6 neighbor pixels. All the EBSD-derived maps, texture-related calculations and plots were performed with MTEX 5.9.0 (Hielscher and Schaeben 2008). The density functions were calculated using the complete EBSD datasets with the de La Vallee Poussin kernel, assuming a half-width of 10 degrees. Low and high angle grain boundaries were calculated assuming a threshold misorientation of 2 and

10 degrees, respectively, and all grains with less than 10 pixels at a minimum were removed from the dataset, but this threshold was varied depending on the sample.

S4.2 EBSD Maps of Starting Material

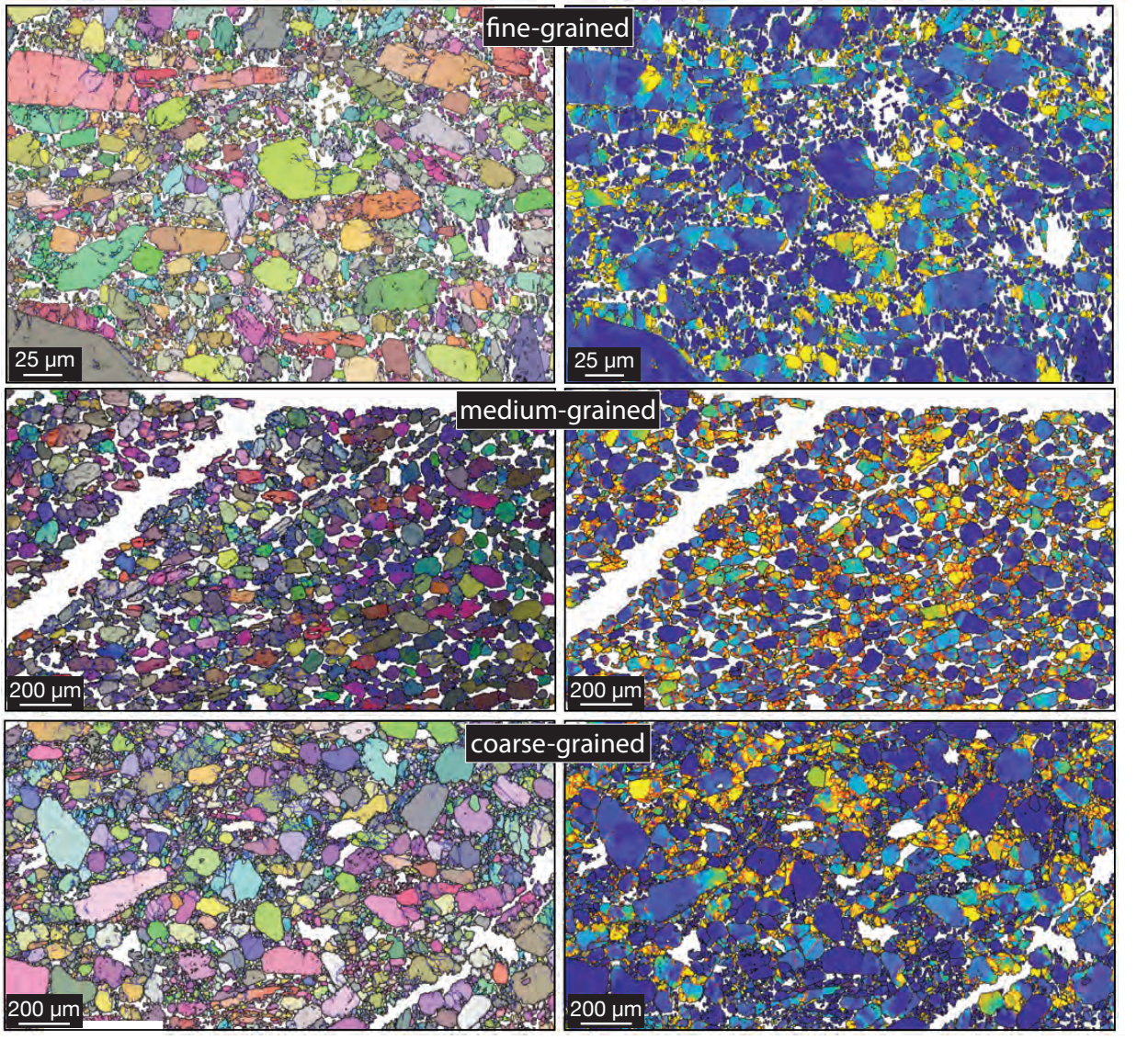

Fine-Grained

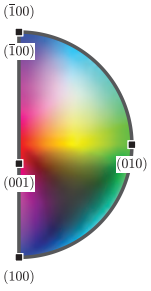

Medium- and Coarse-Grained

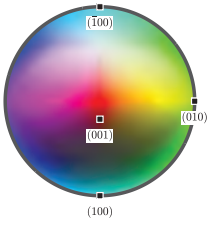

grain boundary (≥10°)
low-angle grain boundary (<10°) for IPFX map
low-angle grain boundary (<10°) for mis2mean map

degrees misorientation

85

Figure S5: Inverse pole figure maps in the X-direction (IPFX maps) and mis2mean maps from the hydrostatic starting material plotted from EBSD data.

References

Donovan, J. J. and Tingle, T. N.: An Improved Mean Atomic Number Background Correction for Quantitative Microanalysis, Microscopy and Microanalysis, 2, 1, doi: 10.1017/S1431927696210013, 1996.

Getsinger, A. J. and Hirth, G.: Amphibole fabric formation during diffusion creep and the rheology of shear zones. Geology, 42 (6): 535–538. doi: 10.1130/G35327.1, 2014.

Hielscher, R. and Schaeben, H.: A novel pole figure inversion method: specification of the MTEX algorithm. J. Appl. Cryst. 41, doi: 10.1107/S0021889808030112, 2008.

Leake, B. E., Woolley, A. R., Arps, C. E. S., Birch, W. D., Gilbert, M. C., Grice, J. D., Hawthorne, F. C., Kato, A., Kisch, H. J., Krivovichev, V. G., Linthout, K., Laird, J., Mandarino, J., Maresch, W. V., Nickel, E. H., Rock, N. M. S., Schumacher, J. C., Smith, D. C., Stephenson, N. C. N., Ungaretti, L., Whittaker, E. J. W., and Youzhi, G.: (1997). Nomenclature of Amphiboles; Report of the Subcommittee on Amphiboles of the International Mineralogical Association Commission on New Minerals and Mineral Names. Mineralogical Magazine, 61(405), 295–310. doi:10.1180/minmag.1997.061.405.13, 1997.

Manthilake, G., Peng, Y., Koga, K.T. et al.: Tracking slab surface temperatures with electrical conductivity of glaucophane. Sci Rep 11, 18014, doi: 10.1038/s41598-021-97317-0, 2021.

Okazaki, K. and Hirth, G.: Deformation of mafic schists from subducted oceanic crust at high pressure and temperature conditions. Tectonophysics, 774, doi: 10.1016/j.tecto.2019.228217, 2020.

Proctor, B. and Hirth, G.: “Ductile to brittle” transition in thermally stable antigorite gouge at mantle pressures. J. Geophys. Res. Solid Earth, 121, 1652–1663, doi:10.1002/2015JB012710, 2016.